Special Issue on Nuclear Science and Technology

ARTICLE

Monte Carlo evaluation of neutron and gamma shielding in coconut shell ash-based concrete drums with borated moderators

Kate Louise P. Francisco*[1], Paul R. Puncia[1,2], Chryzel V. Alano[1,2], Joanna Marie M. Jubelag[3], and Frederick C. Hila[4]

[1]Institute of Physics, College of Arts and Sciences, University of the Philippines Los Baños, College, 4031 Laguna, Philippines
[2]National Institute of Physics, College of Science, University of the Philippines Diliman, 1101 Quezon City, Philippines
[3]Department of Physics, College of Science and Mathematics, Mindanao State University–Iligan Institute of Technology, A. Bonifacio Ave., 9200 Iligan City, Philippines
[4]Applied Physics Research Section, Atomic Research Division, Department of Science and Technology-Philippine Nuclear Research Institute (DOST-PNRI), Commonwealth Ave., Diliman, 1101 Quezon City, Philippines

ABSTRACT

Previous studies have shown that coconut shell ash (CSA)-based concrete outperforms conventional concrete materials used in gamma shielding applications. As CSA is a locally available and abundant aggregate in the Philippines, this study aimed to investigate the neutron and gamma radiation shielding performance of a CSA-based concrete shielding drum paired with borated polyethylene, borated paraffin, and borated water moderators using PHITS. Monte Carlo-based simulations were conducted to calculate ambient dose equivalent rates, $\dot{H}^*(10)$, at the surface and at 1 m from a shielding drum containing an ^{241}Am-Be disused sealed radioactive source. Results indicated that configurations with borated polyethylene yielded total surface and 1 m normalized dose rates of 48.05 ± 0.21 μSv/h/Ci and 1.67 ± 0.02 μSv/h/Ci, respectively. For a 1 Ci source benchmark (Transport Index = 0.17), this places the package strictly into IAEA SSR-6 Category II-YELLOW while complying with IAEA GSR Part 3 occupational dose limits. Although borated polyethylene and borated paraffin demonstrated statistically comparable shielding performance within Monte Carlo uncertainty, borated polyethylene remains the preferred operational choice due to superior structural and thermal stability. The findings highlight the effectiveness of using sustainable CSA-based concrete with various modifiers as radiation-shielding materials.

*Corresponding author
Email Address: **kpfrancisco5@up.edu.ph**
Date received: 31 May 2026
Dates revised: 02 August 2026; 10 August 2026
Date accepted: 17 August 2026
DOI: https://doi.org/10.54645/202619SupFKR-14

INTRODUCTION

Studies on radiation shielding have gained interest in the applied physics field along with the development of nuclear technology, due to the growing demand for safe storage and transport of radioactive materials. Workers in facilities that handle materials of this kind are often exposed to ionizing radiation, which can damage cell structure and cause detrimental effects to their health at high uncontrolled doses (Mohan and Chopra 2022). Recent advances in the design of radiation shielding drums for neutron-gamma sources often involve the use of steel and lead for high-density gamma attenuation, alongside structural concrete and borated materials for combined neutron moderation and absorption (Qi et al. 2022; Zeng et al. 2023). Research on materials that are more effective, accessible, and sustainable for this purpose is therefore of great significance for radiation shielding applications.

A study by Rilwan et al. (2025) experimentally explored the use of coconut shell ash (CSA), a waste material from burning coconut shells, as a partial aggregate in concrete. Their results showed that combining coconut shell ash along with a certain percentage of barite and lime in the concrete mix improved the mechanical and gamma shielding properties of concrete compared to the other concrete mixes under study. This was further supported by the Monte Carlo study of Jubelag et al. (2025), which evaluated the shielding performance of different concretes with locally sourced aggregates for a ^{241}Am-Be neutron source. Their findings suggest that the CSA-based concrete exhibited better gamma shielding

KEYWORDS

borated neutron moderators, CSA-based concrete, dose rate assessment, PHITS, radiation shielding

performance compared to Portland concrete, perlite concrete, and borated concrete. The abundance of CSA in the Philippines and the growing interest in its use as a concrete aggregate make it a promising material for further study. However, limited research has been conducted on the radiation attenuation properties of CSA-based concrete. Its utilization also supports sustainable waste management and resource conservation, underscoring the need to explore its potential applications in radiation shielding (Lejano et al. 2024).

Physicochemically, raw coconut shell ash (CSA) is a pozzolanic material characterized by a high concentration of silica (SiO_2, ~31.2 wt%), potassium oxide (K_2O, ~21.7 wt%), alumina (Al_2O_3, ~17.1 wt%), and trace mineral phases such as quartz, feldspar, and muscovite (Rilwan et al. 2025; Huang et al. 2026). Although raw CSA exhibits a lower specific gravity (~2.06) than Portland cement, modifying the CSA additive with dense minerals like barite ($BaSO_4$) and lime ($Ca(OH)_2$) increases the aggregate mass density to ~2.40 g/cm^3, while enhancing compressive strength and thermal stability via secondary C-S-H gel formation (Rilwan et al. 2025). However, raw CSA's porous particle morphology and high water absorption can reduce mix workability at elevated replacement levels (Lejano et al. 2024; Huang et al. 2026). From a radiation physics perspective, light constituent elements (Si, Al, O, and matrix-bound H) act as effective fast-neutron moderators via elastic scattering, whereas heavy cations (Ba, Ca, Fe) attenuate photons. However, thermal neutron capture (n,γ) on both hydrogen and constituent metallic elements (Fe, K, Ba) produces secondary prompt gamma rays, highlighting the need for coupled neutron-photon transport modeling.

As an extension of the previous study, this study aims to investigate the radiation shielding capabilities of a CSA-based concrete shielding drum with different borated moderators, allowing for a design that effectively shields neutron and gamma radiation. Specifically, it aims to measure the ambient dose equivalent rates at the drum surface and at one meter and compare the neutron–gamma shielding performance of CSA-based concrete when paired with different moderator materials.

Borated materials are often used in radiation shielding due to the high neutron absorption cross-section of boron-10. Meanwhile, materials that primarily contain light elements, such as hydrogen, also serve as moderators. The hydrogen nuclei have a comparable mass to neutrons, making the transfer of kinetic energy to the recoil nuclei more efficient via elastic scattering. This mechanism governs the moderation of fast neutrons to thermal neutrons (Ahmed 2026). In recent studies, the use of composite shielding materials enables both neutron moderation and absorption in a single material, maximizing the neutron-shielding capabilities of systems with design and space constraints (Ahmed 2026; Fu et al. 2021). Accordingly, the borated moderators evaluated in this study are borated polyethylene, borated paraffin, and borated water, which have been used for their neutron shielding capabilities in previous studies (Mortazavi et al. 2016; Hila et al. 2016; Ward and Millero 1974).

Conducting experiments on the radiation-shielding performance of different materials requires substantial resources for synthesizing these materials, determining their chemical composition, and accessing dosimetry equipment, which is usually expensive. Considering this, Monte Carlo simulations offer a more cost-effective and safer method for radiation dose mapping. The Particle and Heavy Ion Transport code System (PHITS) is a Monte Carlo particle simulation code licensed by the Japan Atomic Energy Agency (JAEA) and was developed in collaboration with other institutes (Sato et al. 2023). This transport code can convert particle fluences into operational protection quantities, such as the ambient dose equivalent rate, $\dot{H}^*(10)$, using standard particle- and energy-dependent fluence-to-dose conversion coefficients (Niita et al. 2006). Results from the simulation were then evaluated based on the safety standards of the International Atomic Energy Agency (IAEA 2014a) on the allowable radiation dose relative to the distance from the source in disused sealed radioactive sources. Specifically, the main objective of this study is to evaluate and compare the coupled neutron-gamma radiation shielding performance of a CSA-based concrete drum paired with borated polyethylene, borated paraffin, and borated water moderators for housing a ^{241}Am-Be disused sealed radioactive source. Overall, this study contributes to the development of effective neutron and gamma shielding designs for radiation safety, leveraging computational methods that promote the sustainable use of resources.

MATERIALS AND METHODS

Neutron source, nuclear data library, and PHITS code

A 1 Ci ^{241}Am-Be disused sealed radioactive source (DSRS) was modeled in the central cavity of the drum assembly (Guembou Shouop et al. 2021, 2022). To establish a standardized benchmark, 1 Ci was chosen as an arbitrary source activity to normalize all tally outputs per Ci of ^{241}Am. The source container was modeled according to an industrial X.14-type capsule design (capable of housing source activities up to ~5 Ci), featuring double encapsulation in stainless steel with outer dimensions of 3.0 cm in diameter and 6.0 cm in height, and inner cavity dimensions of 2.52 cm in diameter and 5.05 cm in height. Industrial ^{241}Am-Be sources typically consist of compressed americium dioxide (AmO_2) and beryllium (Be) powder, manufactured with a Be-to-AmO_2 weight ratio of 10:1 to 10:2 (~80–88 wt% ^{241}Am, ~9–17 wt% ^{9}Be, ~3 wt% O) and a compacted powder density of $\rho \approx 1.75$–2.5 g/cm³ (Franco 2014). In this transport model, however, the active cavity interior was defined as air/void. Because primary radiation was sampled directly from the ISO 8529-1:2021 reference emergent spectrum (Annex D), which already incorporates internal energy degradation and self-shielding within standard encapsulated sources, explicitly modeling the physical powder matrix during particle tracking would result in an unphysical double-counting of matrix self-absorption. The total neutron emission rate was scaled with a normalization factor for the source strength, using a value of 2.2 × 10^6 neutrons/s/Ci of ^{241}Am.

To model the coupled neutron-photon radiation field, primary prompt 4.438 MeV gamma rays from the ^{9}Be(α,n)^{12}C* reaction were sampled isotropically throughout the active volume using an evaluated prompt photon-to-neutron emission ratio of $S_\gamma/S_n = 0.575$ (Croft 1989; Liu et al. 2007). Utilizing the ISO reference neutron spectrum alongside the 0.575 gamma yield ratio directly represents the net emergent radiation field exiting standard source capsules, eliminating the need for explicit micro-grain pellet modeling (Croft 1989; Liu et al. 2007). Furthermore, to attenuate the low-energy, high-intensity 59.5 keV primary gamma emissions associated with ^{241}Am decay, a 2-mm thick lead capsule was placed immediately surrounding the double-encapsulated stainless-steel container.

Monte Carlo particle transport simulations were performed using the Particle and Heavy Ion Transport code System (PHITS) version 3.35 to evaluate the neutron and gamma shielding performance of CSA-based concrete drums with borated moderators (Sato et al. 2023; Ogawa 2025). Continuous-energy neutron interaction cross sections were taken from the JENDL-4.0 library (.50c), while photon interaction cross sections were evaluated using the corresponding JENDL-4.0 photo-atomic library (.50p). To

accurately account for chemical binding and molecular thermal motion effects during low-energy neutron scattering ($E < 4$ eV), thermal scattering law $S(\alpha, \beta)$ data at 296.00 K were assigned to hydrogenous materials. Specifically, the $S(\alpha, \beta)$ thermal library for hydrogen in light water (lwtr.20t / H in H_2O) was applied to the bound water within the CSA-based concrete matrix and borated water, while the thermal library for hydrogen in polyethylene (poly.20t / H in Polyethylene) was utilized for both the borated polyethylene and borated paraffin moderator regions.

Shielding drum geometry

A standard 200-L cylindrical storage drum was modeled with a height of 85 cm and a diameter of 57 cm. The drum was constructed as a multilayer shielding system designed to moderate fast neutrons, absorb thermalized neutrons, and attenuate secondary gamma radiation. The layered shielding concept used in the simulation is illustrated in Figure 1.

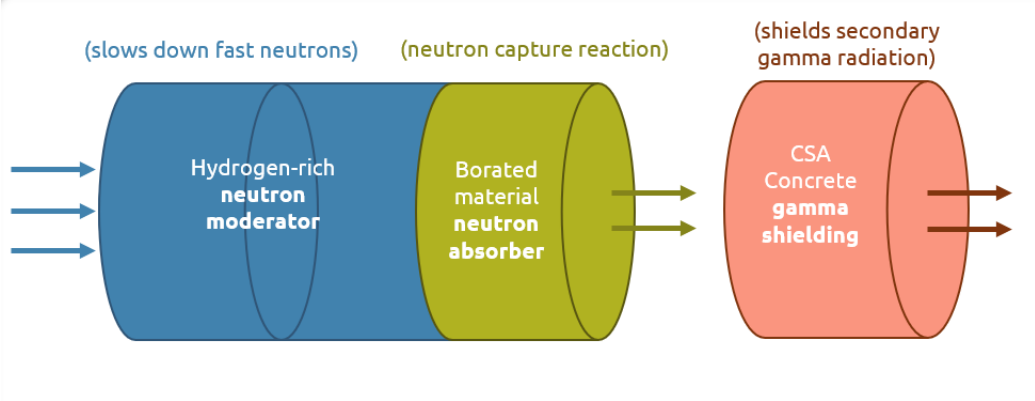

Figure 1: Neutron-shielding framework

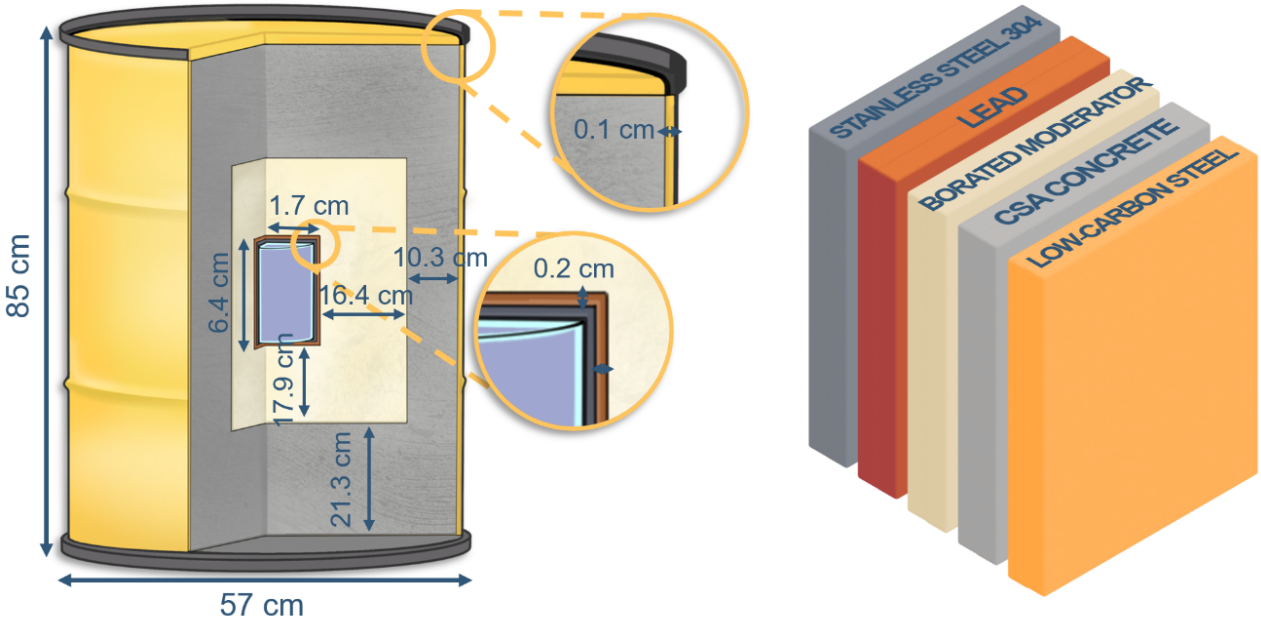

Figure 2: Cross-sectional geometry and dimensions of the shielding drum model.

The shielding structure consisted of several concentric material layers arranged from the innermost to the outermost region. At the center, the ^{241}Am-Be neutron source was enclosed within the stainless steel container measuring 6 cm in external height and 3 cm in external diameter. Surrounding this was a 2 mm-thick lead layer. A 16.4 cm-thick borated moderator region was then placed outside the lead layer to slow down fast neutrons and enhance neutron capture through boron absorption reactions. The remaining layer was filled with the CSA-based concrete, which served as the primary bulk shielding material. The entire assembly was then enclosed within a low-carbon steel drum. The geometric arrangement and layer dimensions used in the PHITS model are shown in Figure 2, which was referenced from Hila et al. (2020) and Nurhadiansyah and Kim (2024). To realistically model ambient atmospheric scattering and transport to the 1-m tally region, the external volume surrounding the shielding drum was explicitly filled with dry sea-level air (composition given in Table 2). The entire physical system was enclosed within a large outer spherical boundary (graveyard) set as an outer transport cutoff cell, beyond which escaping particles were terminated.

Material definitions

Three borated moderator materials were investigated in this study: borated polyethylene, borated paraffin, and borated water. Separate PHITS models were constructed for each moderator configuration to compare their neutron attenuation performance. The elemental compositions and mass densities of the borated moderator materials are summarized in Table 1. Borated polyethylene (1.00 g/cm³) and borated paraffin (0.95 g/cm³) were modeled with 10.0 wt% elemental boron incorporated as B_4C dispersed within their

respective polymer matrices, based on standard formulations in the PNNL Materials Compendium (Detwiler et al. 2021). To reflect physical liquid phase limits, borated water (1.02 g/cm³) was modeled as a saturated aqueous boric acid (H_3BO_3) solution near ambient room temperature conditions (20–25 °C), yielding 0.856 wt% elemental boron (4.89 wt% H_3BO_3), consistent with aqueous solubility data compiled by Crapse and Kyser (2011).

Table 1: Material compositions and densities of the borated moderators.

Material	Density (g/cm³)	Composition (Wt. Fractions)	H Atomic Density (atoms/barn·cm)
Borated Polyethylene*	1.00	H (12.5355%); B (10%); C (77.4645%)	0.074896
Borated Paraffin*	0.95	H (13.3171%); B (10%); C (76.6829%)	0.075587
Borated Water**	1.02	H (11.0223%); B (0.856%); O (88.1217%)	0.067172

*10 wt% elemental boron incorporated as B_4C (boron carbide)

** Saturated H_3BO_3 (boric acid) solution at 25 °C, corresponding to approximately 0.856 wt% elemental boron

The structural and shielding materials used in the drum model, including stainless steel 304, lead, low-carbon steel, air, and CSA-based concrete, were defined separately in the PHITS input file using their respective densities and elemental weight fractions derived from the material compositions summarized in Table 2. The composition and mass density of the CSA-based concrete (CSA-CH-B-0.15, density of 2.40 g/cm³) were adopted from the experimental work of Rilwan et al. (2025). In their study, the optimum CSA-CH-B-0.15 concrete mixture consisted of 0.35 kg Ordinary Portland Cement, 1.0 kg sharp sand, 1.0 kg granite aggregate, and 0.15 kg of lime–barite-modified CSA additive, corresponding to a 30 wt% replacement of cement by the modified additive. The additive consisted of 20 wt% pulverized CSA, 20 wt% $Ca(OH)_2$, and 60 wt% $BaSO_4$. The concrete was prepared using a water-to-cement ratio of 0.5. The density was experimentally determined from measured mass and geometrical volume using the method described by Rilwan et al. (2025), while the chemical composition was characterized by Energy Dispersive X-ray Fluorescence (EDXRF) spectroscopy.

Because EDXRF characterization measures dry elemental oxides and cannot detect light elements such as hydrogen, a standardized hydrogen content was incorporated for neutron transport calculations. In conventional concrete matrices, mineral aggregates act as non-hydrated fillers, while light elements like hydrogen originate primarily from chemically bound water contained within hydration products (such as C-S-H gel and portlandite) (Taylor 1997; Neville 2011). To model a realistic field-cured structural concrete matrix, a baseline hydrogen concentration of 1.0 wt% was assigned, matching the standard Regulatory Concrete specification in the PNNL Materials Compendium (Detwiler et al. 2021). This assignment assumes that in cured matrices, hydrogen density is predominantly governed by initial mix water retention rather than minor variations in dry ash composition. To preserve exact experimental cation stoichiometries from the EDXRF analysis, the dry oxide matrix was scaled to 91.063 wt% to accommodate the 8.937 wt% equivalent bound water (1.000 wt% H and 7.937 wt% O).

Table 2: Material compositions and densities of other materials.

Material	Density (g/cm³)	Composition (Wt. Fractions)
Air (dry, near sea level)	0.001205	C (0.0124%); N (75.5268%); O (23.1781%); Ar (1.2827%)
Concrete, CSA-Based	2.4	H (1%); O (44.815%); Mg (0.632%); Al (5.685%); Si (18.377%); P (0.089%); S (0.43%); K (0.849%); Ca (19.756%); Ti (0.202%); Mn (0.166%); Fe (1.682%); Sr (5.054%); Ba (0.972%)
Lead	11.35	Pb (100%)
Steel, Low Carbon (1008)	7.872	C (0.1%); P (0.04%); S (0.05%); Mn (0.5%); Fe (99.31%)
Steel, Stainless (304)	8.03	C (0.08%); Si (1%); P (0.045%); S (0.03%); Cr (19%); Mn (2%); Fe (68.345%); Ni (9.5%)

Simulation parameters

Monte Carlo particle transport calculations were performed using 2.0×10^7 source particle histories, divided into 20 independent simulation batches (10^6 histories per batch) for statistical reliability. Statistical convergence and batch-to-batch consistency were evaluated by tracking tally relative error as a function of simulated histories. For all primary surface and 1-m region tallies, the fractional relative standard error (R) satisfied $R < 0.015$ (1.5%), well below the established Monte Carlo convergence threshold of $R < 0.05$. Particle tallies exhibited monotonic $1/N^{1/2}$ variance reduction across all 20 batches without outlier trends, confirming spatial and energy convergence of the simulated radiation field.

The neutron transport energy range was defined from 10^{-11} MeV to 20 MeV to fully encompass the thermal regime and the maximum emission energies of the source. The initial energy spectrum for the Am-Be neutron source was defined according to the standard 8529-1 set by the International Organization for Standardization (ISO 2021) for reference radiation fields, as depicted in Figure 3. For each moderator configuration, identical geometric and source parameters were used to ensure that observed differences in shielding performance were due only to the moderator material properties.

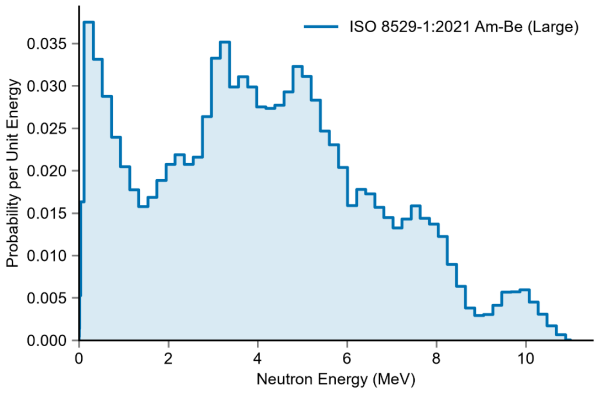

Figure 3: Energy spectrum of the Am-Be neutron source as defined by the ISO 8529-1:2021 standard (ISO 2021), utilized as the source definition in the Monte Carlo simulations.

Radiation transport tallies

Radiation transport through the shielding system was evaluated using the [T-TRACK] tally with a region mesh configuration in PHITS. This tally records the particle track length within specified spatial regions, allowing the calculation of particle fluence and operational radiation protection quantities. To map the surface and 1-m dose rate distributions, cell regions acting as detectors were defined by axially slicing thin cylindrical layers (specifically, the outermost low-carbon steel layer for the drum surface, and a 1-cm thick air boundary at a 1-m radial offset) into a series of stacked ring cells. For internal radial dose profiles, the drum volume was embedded with a series of concentric cylindrical rings of increasing diameter. Particle track length fluences within each declared tally cell were converted into the ambient dose equivalent rate, $\dot{H}^*(10)$, in units of μSv/h per Ci of ^{241}Am, using energy-dependent conversion multipliers from the EXPACS database embedded within PHITS version 3.35. These multipliers utilize the fluence-to-ambient-dose-equivalent conversion coefficients from ICRP Publication 74 for neutrons below 200 MeV and standard PHITS-calculated conversion factors for photons (ICRP 1996; Sato 2016, 2018). The detector regions surrounding the shielding drum recorded the resulting dose rate distributions for escaping neutrons as well as primary and secondary gamma photons.

Data analysis

The calculated dose distributions for each moderator configuration were extracted from the PHITS output files and analyzed to evaluate shielding performance. All maximum dose rates reported in this study were extracted directly from the raw mesh tally bins together with their propagated standard uncertainties (±1σ). For continuous spatial visualization across axial profile plots, the raw tally distributions were fitted using an empirical modified Lorentzian profile tailored for peak plateau broadening and algebraic scattering tails. Uncertainty bands (1σ) for these visual model curves were computed via Jacobian matrix propagation of the spatial dose rate variance. These continuous fitted profiles are used solely to illustrate spatial attenuation trends among the three moderator materials, while all quantitative comparisons and regulatory assessments rely strictly on raw tally maxima.

Model Benchmarking and Validation

To validate the radiation transport physics and tallies implemented in PHITS 3.35, an independent Monte Carlo benchmark calculation was conducted using MCNP5 (X-5 Monte Carlo Team 2003). The optimal drum geometry featuring the borated polyethylene moderator and CSA-based concrete layer was modeled with identical dimensions, material compositions, densities, and source specifications. MCNP5 performed particle transport using the ENDF/B-VII.0 evaluated library (.70c) for continuous-energy neutrons, paired with the MCPLIB04 photo-atomic data library (.04p, derived from EPDL97) for photon transport. Particle fluences in MCNP5 were converted to ambient dose equivalent rates, $\dot{H}^*(10)$, using ICRP Publication 74 (ICRP 1996) conversion functions for neutrons and EXPACS (Sato 2016, 2018; Sato et al. 2023) conversion multipliers for photons, matching the dosimetric quantities evaluated in PHITS.

RESULTS AND DISCUSSION

Surface Neutron and Photon Ambient Dose Equivalent Rates

Statistical reliability of the Monte Carlo calculations was verified through batch convergence testing across 2.0×10^7 source particles. Direct source photon tallies achieved relative errors of $R \leq 0.72\%$, while peak surface neutron and secondary photon dose rate tallies converged to relative standard errors of $R \leq 1.42\%$ and $R \leq 1.50\%$, respectively. All reported dose rates in Tables 3 and 4 explicitly include propagated absolute uncertainties (±1σ), and figures incorporate corresponding 1σ uncertainty bars and model confidence bands.

In order to determine the most effective neutron-gamma shielding configuration, the neutron and photon ambient dose equivalent rates at the surface of the shielding drum were evaluated for the three borated moderator configurations. To quantitatively assess the radiation behavior, the spatial dose profiles from the simulations were fitted using an empirical modified Lorentzian function tailored for peak plateau broadening and algebraic scattering tails.

Figure 4 shows the neutron ambient dose equivalent rates at the drum surface for three different moderator configurations: borated paraffin, borated polyethylene, and borated water. The surface neutron profiles reveal distinct variations in shielding efficiency driven by the moderating materials. The configuration using borated polyethylene yielded the lowest peak surface total neutron ambient dose equivalent rate of 44.91 ± 0.21 μSv/h/Ci (dominated by fast neutrons at 43.87 ± 0.21 μSv/h/Ci). Meanwhile, the borated paraffin configuration produced a slightly higher peak value than borated polyethylene, at 45.75 ± 0.21 μSv/h/Ci, indicating that its neutron attenuation performance was comparable under the simulated geometry. This suggests that both materials exhibited similar shielding effectiveness, with only minor differences observed in the resulting dose. Borated water, on the other hand, produced the highest surface neutron ambient dose equivalent rate among the three cases at 63.01 ± 0.24 μSv/h/Ci, indicating that the configuration with borated water as the moderator had the least effective neutron-shielding performance in the present drum geometry. The nearly identical performance of borated polyethylene and paraffin can be attributed to their chemical composition. Both materials are hydrogen-rich and therefore promote fast-neutron moderation through elastic scattering with hydrogen nuclei. The added boron then enhances thermal-neutron absorption after moderation (Gokul et al. 2023). The lower neutron dose rates observed for borated polyethylene (44.91 ± 0.21 μSv/h/Ci) and borated paraffin (45.75 ± 0.21 μSv/h/Ci) compared to borated water (63.01 ± 0.24 μSv/h/Ci) can be directly attributed to their higher hydrogen atomic densities (0.0749 and 0.0756 atoms/barn·cm vs. 0.0672 atoms/barn·cm), which enhance fast-neutron moderation via elastic scattering, combined with their higher boron loading (10.0 wt% vs. 0.856 wt%) for thermal neutron capture.

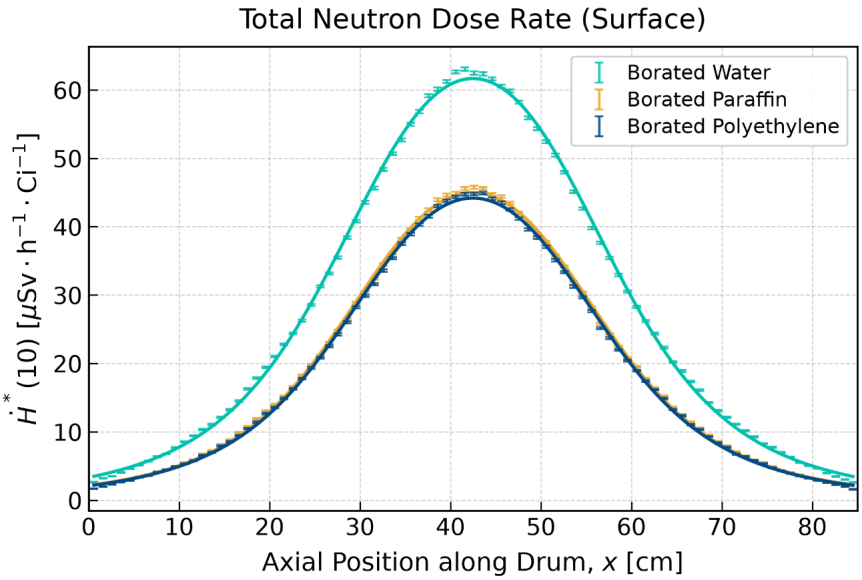

Figure 4: Superimposed empirical model fittings of the neutron ambient dose equivalent rates at the surface.

When evaluated alongside their associated Monte Carlo statistical uncertainties (±1σ), the surface neutron ambient dose equivalent rates for borated polyethylene (44.91 ± 0.21 μSv/h/Ci) and borated paraffin (45.75 ± 0.21 μSv/h/Ci) differ by only 1.8%. Because this marginal variation falls within the combined 2σ statistical uncertainty bounds, their radiation attenuation capabilities are statistically comparable, aligning with recent shielding and moderation studies where selection criteria extend beyond marginal computational dose differences to practical engineering trade-offs (Zeng et al. 2023; Qi et al. 2022). From a material practicality standpoint, borated polyethylene is preferable for long-term storage applications because of its higher thermal stability, improved dimensional and mechanical stability, and superior resistance to deformation compared with low-melting paraffin. It also avoids the leakage and evaporation concerns associated with liquid moderators such as borated water.

Figure 5 illustrates the photon ambient dose equivalent rates at the surface. The photon profiles provide an additional measure of shielding performance by showing the extent to which primary source photons (γ_{src}) and secondary photons (γ_{sec}) generated in the moderator and concrete are attenuated before reaching the drum surface. The total surface photon dose rates ($\gamma_{src} + \gamma_{sec}$) followed the same observed order, with borated polyethylene and paraffin giving the lowest ambient dose equivalent rates. Notably, the photon dose rates for both materials were nearly overlapping, with maximum total surface photon dose rates of 3.141 ± 0.007 μSv/h/Ci for borated polyethylene (γ_{src} = 2.358 ± 0.005, γ_{sec} = 0.783 ± 0.004 μSv/h/Ci) and 3.180 ± 0.007 μSv/h/Ci for borated paraffin (γ_{src} = 2.392 ± 0.005, γ_{sec} = 0.795 ± 0.004 μSv/h/Ci). Borated water yielded a slightly higher total surface photon dose rate of 3.311 ± 0.007 μSv/h/Ci (γ_{src} = 2.333 ± 0.005, γ_{sec} = 0.983 ± 0.004 μSv/h/Ci). Note that because the component and total values represent independent spatial maxima along the drum's height that do not strictly coincide in position, the sum of the individual component peaks differs slightly from the reported total. The modified CSA-based concrete reduced the secondary photon field after the moderator layer, consistent with the expected photon-attenuation contribution of dense mineral additives such as barite (Gokul et al. 2023). Based on the peak surface ambient dose equivalent rates, borated polyethylene was selected as the best-performing moderator among the three materials tested.

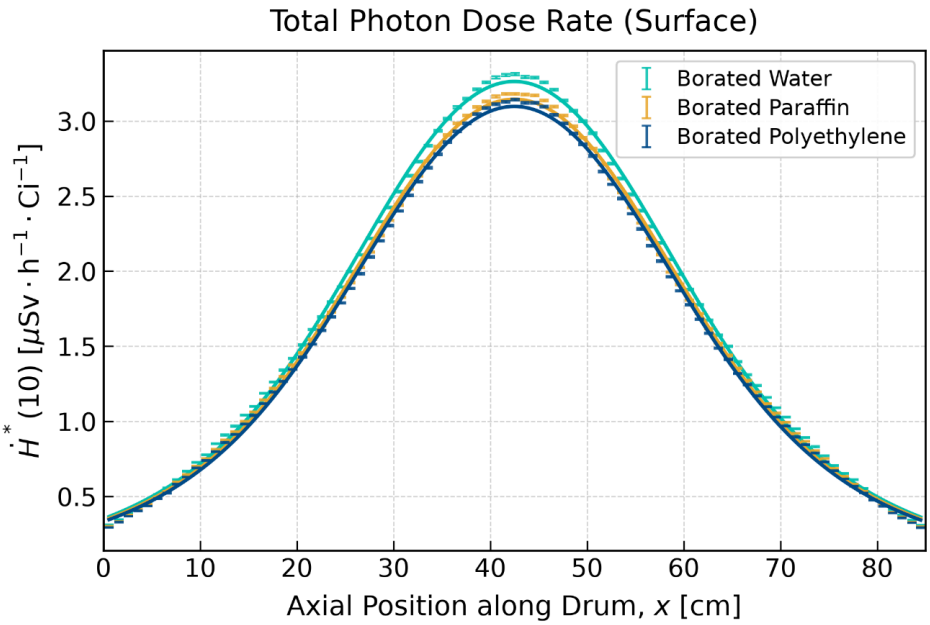

Figure 5: Superimposed empirical model fittings of the photon ambient dose equivalent rates at the surface.

Internal Neutron and Photon Ambient Dose Equivalent Rate Trends Across Shielding Layers

Having identified the most effective configuration of the shielding drum, we further investigated its internal shielding mechanisms within the different layers. Figure 6 illustrates the radial distribution of ambient dose equivalent rates for neutrons, primary source photons (γ_{src}), secondary capture photons (γ_{sec}), and total radiation as a function of distance from the center of the drum. As the neutrons emitted from the ^{241}Am-Be source enter the borated polyethylene layer (1.7-18.1 cm), the neutron ambient dose equivalent rate decreases approximately exponentially with radial distance. This continuous neutron attenuation is driven by elastic scattering in the hydrogen-rich polyethylene material, which moderates fast neutrons, followed by thermal-neutron absorption in boron-10 (Dymova et al. 2020).

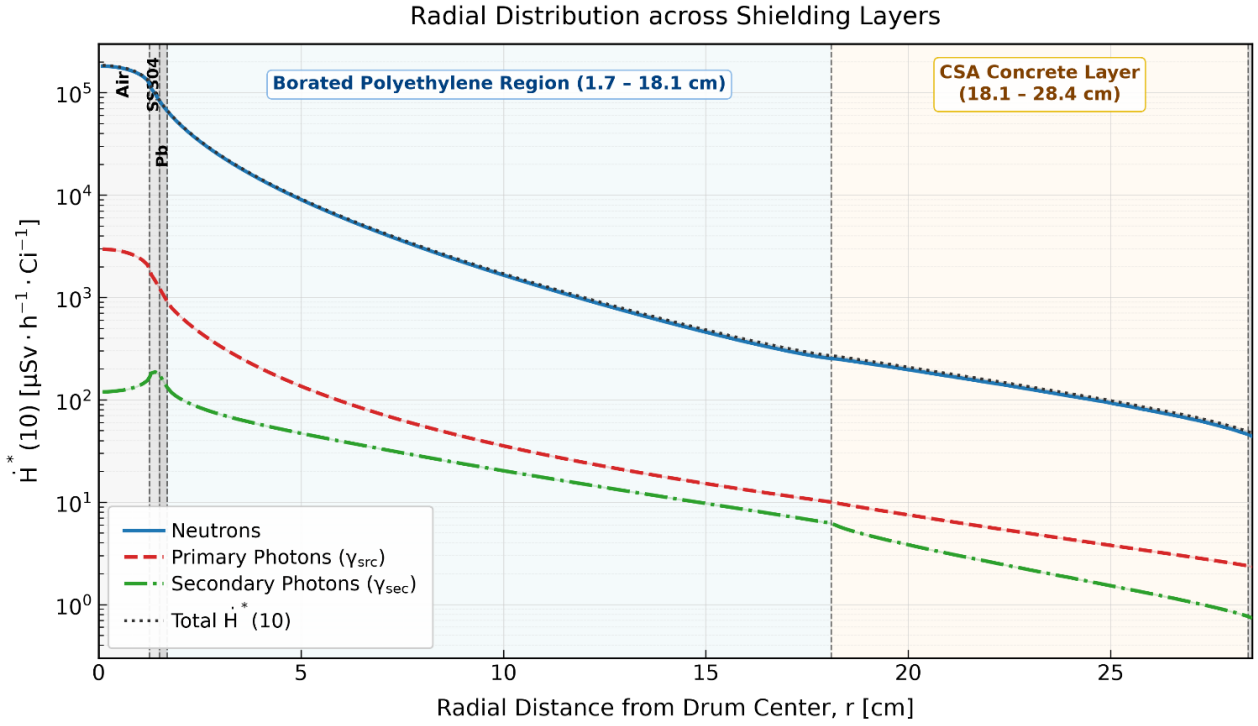

Figure 6: Radial ambient dose equivalent rate profiles for neutrons, primary photons (γsrc), secondary photons (γsec), and total radiation across concentric shielding layers of the optimized drum configuration.

In the inner capsule and sheath regions ($r < 1.7$ cm), the secondary photon dose rate exhibits an initial build-up peak, reaching its maximum at $r = 1.40$ cm due to inelastic scattering and radiative capture in the structural materials. Upon entering the borated polyethylene layer, the secondary photon contribution transitions to a steady downward trend across the moderator thickness. As the photon field traverses the CSA-based concrete layer (18.1-28.4 cm), both primary and secondary photon dose rates continue to

attenuate exponentially across the concrete thickness. This behavior confirms that the CSA-based concrete layer contributes significantly to photon attenuation, particularly through the increased density and photon-interaction probability associated with barite addition (Gokul et al. 2023). It acts as an effective outer barrier for the remaining high-energy photons before they can escape the drum surface.

To visualize the spatial attenuation of the radiation field, 2D mesh distributions of the ambient dose equivalent rates were generated for the optimal configuration (borated polyethylene and CSA-based concrete). Figure 7 illustrates the cross-sectional heatmaps for (a) neutrons, (b) primary 4.438 MeV photons, and (c) secondary photons. The visual contours demonstrate strong attenuation and spatial reduction of the neutron field within the internal moderating layers, alongside substantial shielding of both primary source photons and secondary capture gammas through the bulk CSA-based concrete.

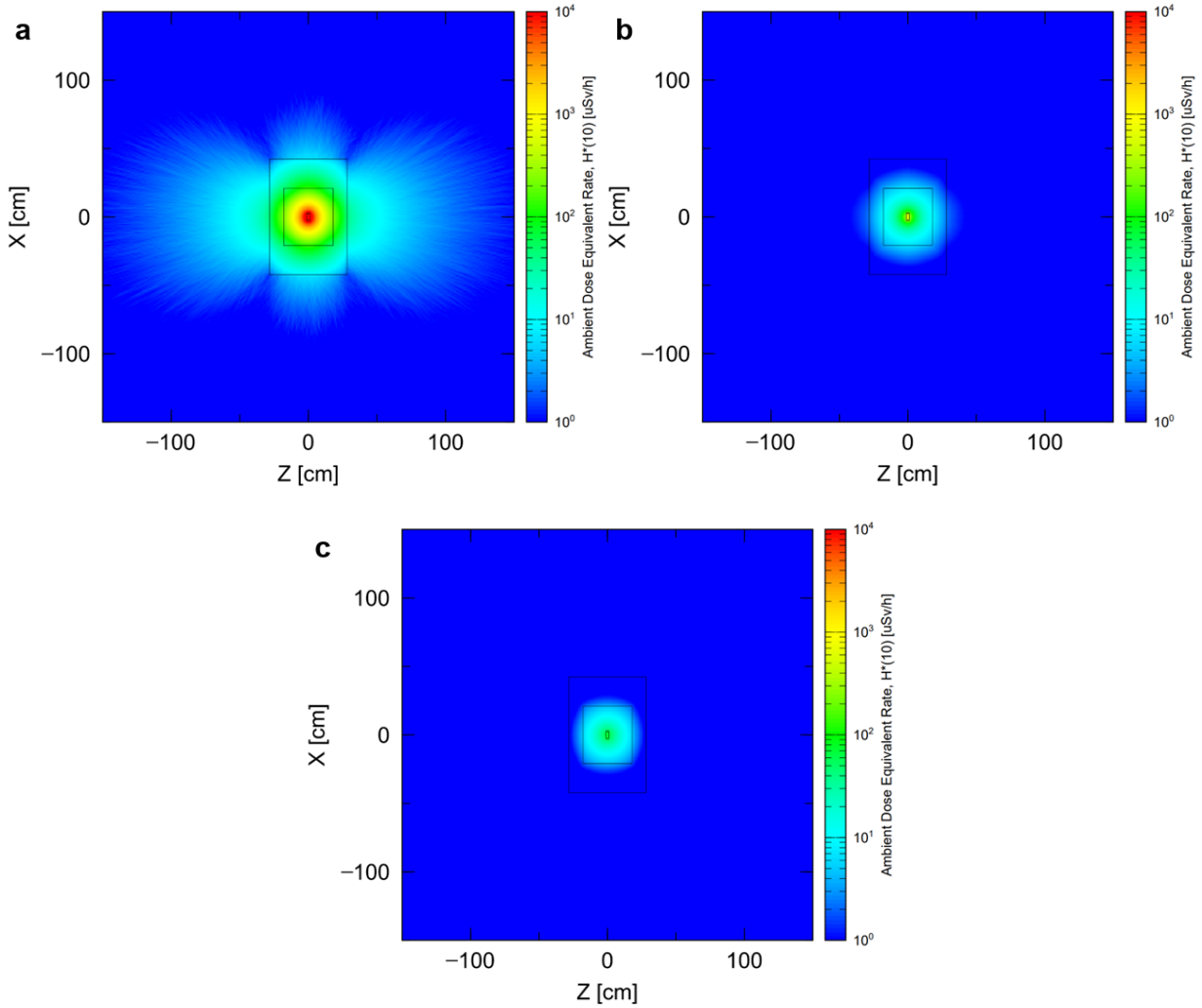

Figure 7: Cross-sectional 2D heatmaps of the (a) neutron, (b) primary 4.438 MeV photon, and (c) secondary photon ambient dose equivalent rates (μSv/h per Ci 241Am-Be source) for the optimized shielding configuration consisting of borated polyethylene and CSA-based concrete layers.

Peak Ambient Dose Equivalent Rates at the Surface and at a 1-Meter Distance

To evaluate the practical shielding performance of the drum for storage and handling of a ^{241}Am-Be source, the peak neutron and photon ambient dose equivalent rates were extracted at the drum surface and at a radial distance of 1 m from the drum surface. Table 3 and Table 4 summarize the peak neutron and photon ambient dose equivalent rates for the drum configurations utilizing the three different borated moderators.

Table 3: Summary of Maximum Neutron Ambient Dose Equivalent Rates at the Surface and 1-Meter Away from the Drum

Detector Location	Neutron Moderator	Maximum Neutron Ambient Dose Equivalent Rate (μSv/h/Ci)			
		Thermal (<0.5 eV)	Epithermal (0.5 eV– 100 keV)	Fast (>100 keV)	Total
At Surface of the Drum	Borated Water	0.468±0.004	1.112±0.011	61.44±0.24	63.01±0.24
	Borated Paraffin	0.238±0.003	0.833±0.009	44.68±0.21	45.75±0.21
	Borated Polyethylene	0.236±0.003	0.818±0.009	43.87±0.21	44.91±0.21
1-m from Surface of the Drum	Borated Water	0.0137±0.0002	0.0329±0.0007	2.167±0.021	2.212±0.021
	Borated Paraffin	0.0073±0.0002	0.0232±0.0006	1.537±0.017	1.566±0.017

Detector Location	Neutron Moderator	Maximum Neutron Ambient Dose Equivalent Rate (μSv/h/Ci)			
		Thermal (<0.5 eV)	Epithermal (0.5 eV– 100 keV)	Fast (>100 keV)	Total
	Borated Polyethylene	0.0071±0.0002	0.0228±0.0006	1.504±0.016	1.532±0.017

Table 4: Summary of Maximum Photon Ambient Dose Equivalent Rates at the Surface and 1-Meter Away from the Drum

Detector Location	Neutron Moderator	Maximum Photon Ambient Dose Equivalent Rate (μSv/h/Ci)		
		Direct Source	Neutron-induced	Total
At Surface of the Drum	Borated Water	2.333±0.005	0.983±0.004	3.311±0.007
	Borated Paraffin	2.392±0.005	0.795±0.004	3.180±0.007
	Borated Polyethylene	2.358±0.005	0.783±0.004	3.141±0.007
1-m from Surface of the Drum	Borated Water	0.1073±0.0005	0.0367±0.0004	0.1436±0.0006
	Borated Paraffin	0.1106±0.0006	0.0301±0.0003	0.1402±0.0006
	Borated Polyethylene	0.1089±0.0006	0.0298±0.0003	0.1382±0.0006

As shown in Tables 3 and 4, the borated polyethylene and CSA-based concrete configuration produced the lowest peak neutron and photon ambient dose equivalent rates at 1 m from the surface, with values of 1.532 ± 0.017 μSv/h and 0.1382 ± 0.0006 μSv/h, respectively. Under the simulated source strength and geometry, it produced a combined total ambient dose equivalent rate of 1.671 ± 0.017 μSv/h at 1 m. These values indicate substantial attenuation of both the primary neutron and associated photon radiation.

To assess the regulatory compliance and transport categorization of the drum containing a 1 Ci ^{241}Am-Be source, the calculated ambient dose equivalent rates were evaluated against IAEA SSR-6 (Regulations for the Safe Transport of Radioactive Material) (IAEA 2025) package criteria. Package categories are determined by the maximum surface ambient dose equivalent rate and the Transport Index (TI), defined as the dose rate in mrem/h at 1 m from the outer surface (TI = $\dot{H}^*(10)$ at 1 m / 10 μSv/h , where 1 mrem/h ≡ 10 μSv/h). For the optimal configuration utilizing borated polyethylene and CSA-based concrete, the maximum combined (neutron + photon) ambient dose equivalent rates are 48.05 ± 0.21 μSv/h at the surface and 1.67 ± 0.02 μSv/h at 1 m (TI = 0.17). Because the surface dose rate exceeds 5 μSv/h and the 1 m dose rate yields a TI ≤ 1.0, the package falls strictly into Category II-YELLOW (TI ≤ 1.0, surface dose rate ≤ 500 μSv/h).

Parametric calculations of maximum allowable ^{241}Am-Be source strength based on IAEA SSR-6 limits demonstrate that the borated polyethylene shielding drum can accommodate up to 0.104 Ci for Category I-WHITE (governed by the 5 μSv/h surface limit), 5.99 Ci for Category II-YELLOW (governed by the TI limit of 10 μSv/h at 1 m), 41.62 Ci for Category III-YELLOW non-exclusive use (governed by the 2000 μSv/h surface limit), and 119.72 Ci under Category III-YELLOW exclusive use, as illustrated in Figure 8.

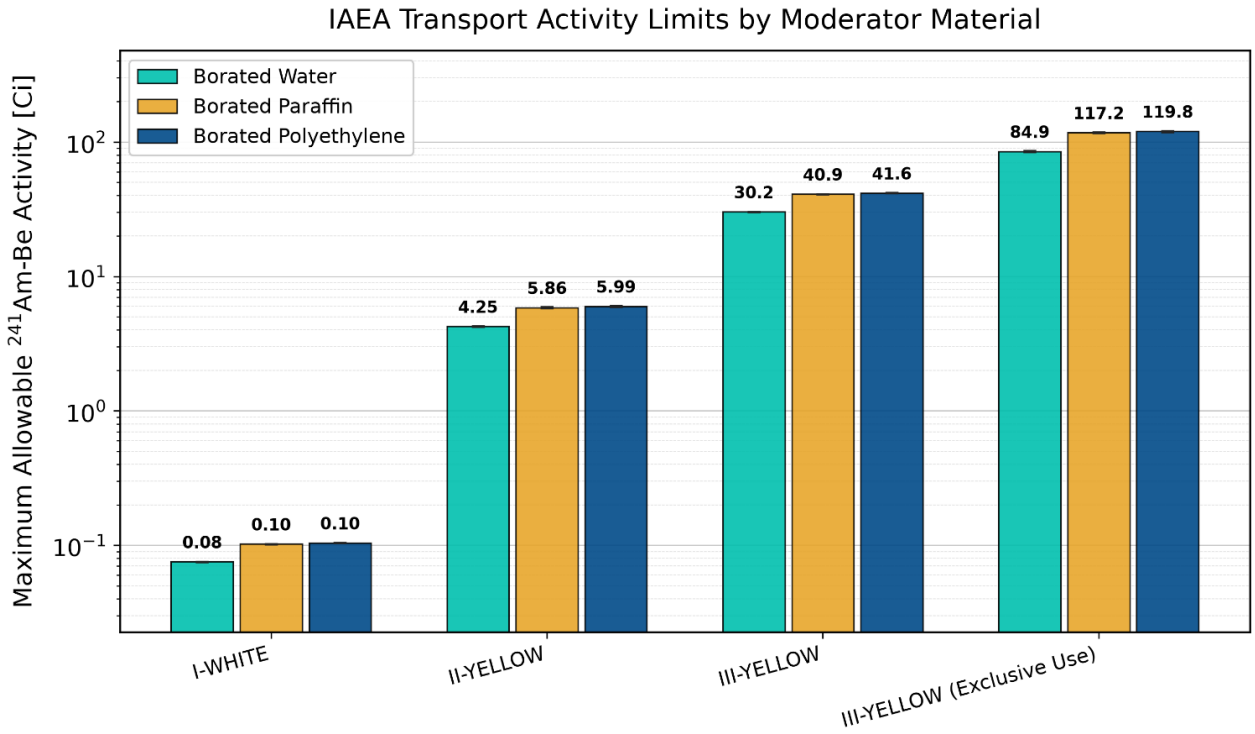

Figure 8: Maximum allowable 241Am-Be source activity (Ci) across IAEA SSR-6 transport package categories (Category I-WHITE, Category II-YELLOW, Category III-YELLOW, and Category III-YELLOW Exclusive Use) for shielding drum configurations utilizing borated polyethylene, borated paraffin, and borated water moderators.

For stationary storage applications governed by IAEA GSR Part 3 (Radiation Protection and Safety of Radiation Sources: International Basic Safety Standards) (IAEA 2014b), compliance is determined by occupational and public dose limits rather than

transport package categories. Assuming a conservative occupational exposure scenario where a worker spends a full working year (2000 hours/year) at a distance of 1 m from a drum loaded with a 1 Ci ^{241}Am-Be source ($\dot{H}^*(10)$ = 1.67 μSv/h), the cumulative annual occupational dose accrued would be ~3.34 mSv/year, which remains well within the IAEA GSR Part 3 occupational effective dose limit of 20 mSv/year.

The multi-layer drum approach evaluated in this study aligns with established storage configurations in the literature, such as the lead, polyethylene, and Ordinary Portland Concrete (OPC) system modeled by Nurhadiansyah and Kim (2024) for ^{241}Am-Be sources. Building upon this foundational geometric layout, the present work demonstrates that integrating 10.0 wt% boron doping into the moderating layer alongside CSA-based concrete effectively manages thermalized neutrons and secondary photons, maintaining low ambient dose equivalent rates (48.05 ± 0.21 μSv/h per Ci at the surface).

Monte Carlo Code Benchmarking (PHITS vs. MCNP5)

The comparison between PHITS 3.35 and MCNP5 for the optimized borated polyethylene configuration demonstrates high dosimetric consistency across all individual radiation components as well as total combined dose rate profiles. As shown in Figure 9 (top), the spatial attenuation profiles for primary neutrons, secondary capture photons (γ_{sec}), and direct source photons (γ_{src}) calculated by both codes exhibit near-identical spatial trends and magnitudes. For the combined total ambient dose equivalent rate (Figure 9 (bottom)), the mean absolute percentage error (MAPE) between PHITS and MCNP5 across all axial positions is 3.16% at the drum surface (RMSE = 0.68 μSv/h) and 2.86% at 1 m distance (RMSE = 0.05 μSv/h). Furthermore, 65.9% of spatial bins at the surface and 83.5% of spatial bins at 1 m lie within the combined 2σ statistical confidence intervals. Minor deviations are likely attributable to differences in underlying nuclear data libraries (JENDL-4.0 in PHITS vs. ENDF/B-VII.0 in MCNP5). This close quantitative agreement validates the accuracy and implementation of the shielding drum model in PHITS.

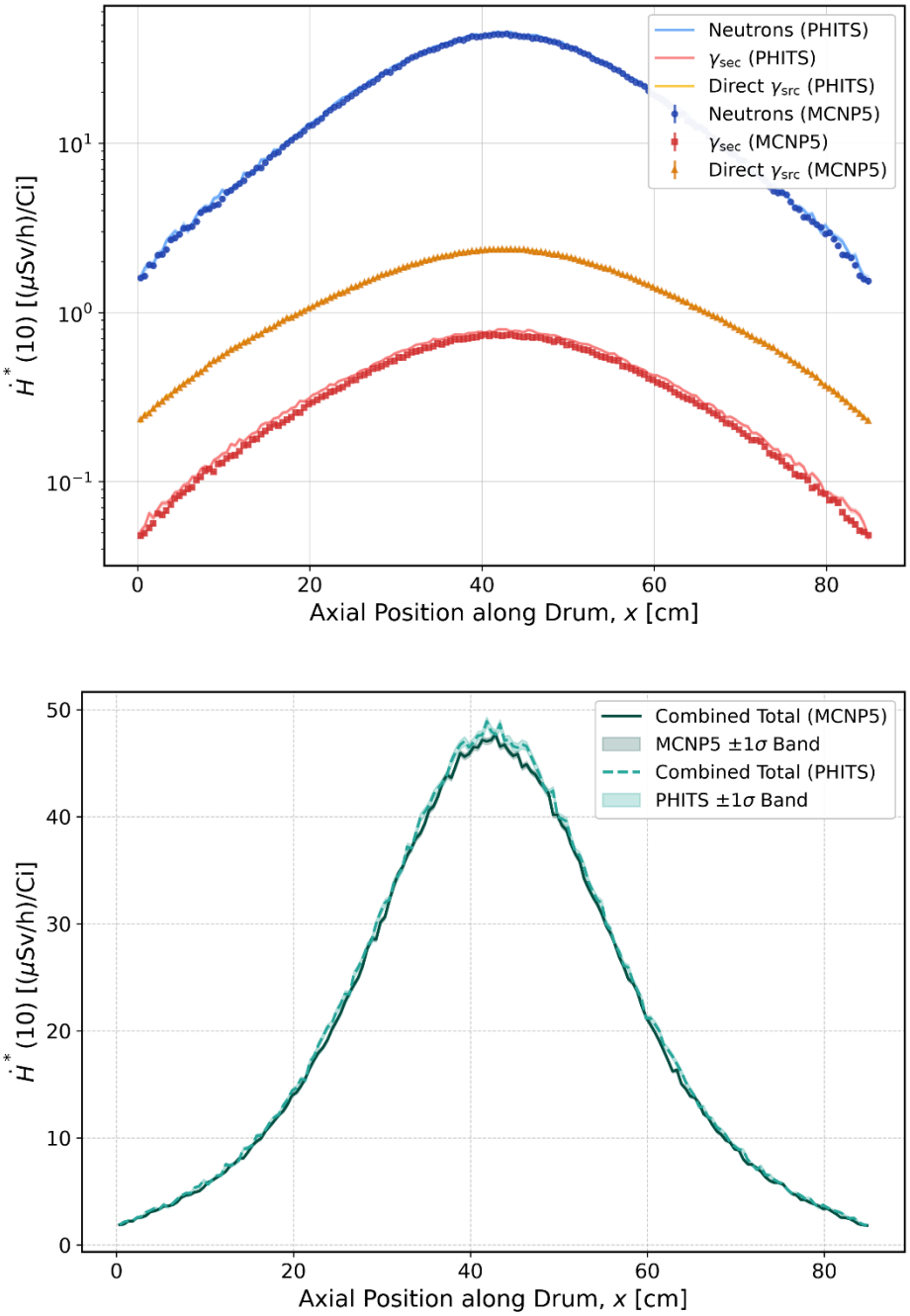

Figure 9: Comparison of PHITS 3.35 and MCNP5 axial ambient dose equivalent rate profiles for the optimized shielding drum: (top) primary neutrons, secondary capture gamma rays, and source gamma rays; (bottom) total ambient dose equivalent rate with ±1σ uncertainty bands.

CONCLUSION

This study demonstrated that the use of CSA-based concrete with three different boron-rich neutron moderators yielded ambient dose equivalent rates, $\dot{H}^*(10)$, that me t IAEA Transport Regulation (SSR-6 Category II-YELLOW) and storage safety limits both at the surface and at a 1-meter distance. Neutron dose rates significantly decreased upon interacting with hydrogen- and boron-rich materials via elastic scattering and neutron capture reactions. Despite an initial increase in secondary photon dose rates near the lead and neutron moderator layers due to radiative capture emissions, shielding effects ultimately dominated , resulting in effective attenuation of both neutron and photon radiation. The CSA-based concrete and borated polyethylene configuration yielded the lowest normalized dose rates (48.05 ± 0.21 μSv/h/Ci at surface; 1.67 ± 0.02 μSv/h/Ci at 1 m), showing statistically comparable shielding performance to borated paraffin within Monte Carlo uncertainty while offering superior thermal and mechanical stability. Overall, these findings reinforce the potential of CSA-based concrete as a sustainable shielding material and its possible applications in future radioactive storage systems.

ACKNOWLEDGMENTS

This work was primarily funded and monitored by DOST-Philippine Council for Industry, Energy, and Emerging Technology Research and Development (DOST-PCIEERD) with

Project No. 1213067, 2025. The authors acknowledge the Applied Physics Research Section (APRS) of the DOST-Philippine Nuclear Research Institute (DOST-PNRI) for providing the MCNP5-generated simulation data used for code validation in this study.

CONFLICT OF INTEREST

The authors declare that there is no conflict of interest.

REFERENCES

Ahmed GSM. Neutron shielding: advanced mechanisms, challenges, and material strategies. Radiat Phys Chem 2026; 241:113544.

Crapse KP, Kyser EA III. Literature review of boric acid solubility data. Report SRNL-STI-2011-00578. Aiken: Savannah River National Laboratory, 2011.

Croft S. The use of neutron intensity calibrated ^{9}Be(α, n) sources as 4438 keV gamma-ray reference standards. Nucl Instrum Methods Phys Res A 1989; 281(1):103–116.

Detwiler RS, McConn RJ, Grimes TF, Upton SA, Engel EJ. Compendium of material composition data for radiation transport modeling. Pacific Northwest National Laboratory 2021; PNNL-15870 Rev. 2.

Dymova MA, Taskaev SY, Richter VA, Kuligina EV. Boron neutron capture therapy: current status and future perspectives. Cancer Commun 2020; 40(9):406– 421.

Franco M. Characterization of the neutron irradiation system for use in the low-dose-rate irradiation facility at Sandia National Laboratories. Report SAND2014-16188. Albuquerque: Sandia National Laboratories, 2014.

Fu X, Ji Z, Lin W, Yu Y, Wu T. The advancement of neutron shielding materials for the storage of spent nuclear fuel. Sci Technol Nucl Install 2021; 2021.

Gokul P, Ashok Kumar J, Preetha R, Chattopadhyaya S, Mini KM. Additives in concrete to enhance neutron attenuation characteristics – a critical review. Results Eng 2023; 19:101281.

Guembou Shouop CJ, Ndontchueng Moyo M, Nguelem Mekongtso EJ, Beyala Ateba JF, Strivay D. 241Am/Be source optimum geometry for DSRS management-based Monte Carlo simulations. AIP Adv 2021; 11(11):115206.

Guembou Shouop CJ, Mbida Mbembe S, Tayou Kamkumo C, Beyala Ateba JF, Ndontchueng Moyo M, Nguelem Mekongtso EJ, Simo A, Strivay D. Monte Carlo optimum management of 241Am/Be disused sealed radioactive sources. Sci Rep 2022; 12(1):1511.

Hila FC, Jecong JF, Dingle C, Lopez G, Romallosa K, Guillermo N. Design of a semiportable shielding for a CF-252 neutron source using MCNP-5. Proceedings of the 36th Samahang Pisika ng Pilipinas Physics Conference 2016.

Hila FC, Piquero RE, Dingle CAM, Astronomo AA, Jecong JFM, Marcelo EA. Dose rate analysis of upgraded storage drums for disused sealed radioactive sources by a multivariate interpolation program developed using MCNP5. Philipp J Sci 2020; 149(S1):65– 75.

Huang F, Peng D, Zhao Y, Zhao G, Fu S. Effects of coconut shell ash and coir fiber on the mechanical properties and microstructure of concrete. Buildings 2026; 16(5):1063.

[IAEA] International Atomic Energy Agency. Management of disused sealed radioactive sources. Vienna: International Atomic Energy Agency, 2014a.

[IAEA] International Atomic Energy Agency. Radiation protection and safety of radiation sources: international basic safety standards. IAEA Safety Standards Series No. GSR Part 3. Vienna: International Atomic Energy Agency, 2014b.

[IAEA] International Atomic Energy Agency. Regulations for the safe transport of radioactive material. IAEA Safety Standards Series No. SSR-6 (Rev. 2). Vienna: International Atomic Energy Agency, 2025.

[ICRP] International Commission on Radiological Protection. Conversion Coefficients for use in Radiological Protection against External Radiation. ICRP Publication 74. Ann ICRP 1996; 26(3-4):1–205.

[ISO] International Organization for Standardization. Neutron reference radiation fields—Part 1: characteristics and methods of production (ISO 8529-1:2021). 2021.

Jubelag JM, Francisco KP, Alano CV, Puncia PR, Hila FC. Monte Carlo-based assessment of concrete shielding drums with locally-sourced aggregates for ^{241}Am-Be neutron source. Proceedings of the 27th National SPVM Physics Conference 2025.

Lejano B, Elevado KJ, Fandiño MA, Ng EA, Datinguinoo ZAN, Oliveros SB. Experimental investigation of utilizing coconut shell ash and coconut shell granules as aggregates in coconut coir reinforced concrete. Clean Eng Technol 2024; 21:100779.

Liu Z, Chen J, Zhu P, Li Y, Zhang G. The 4.438MeV gamma to neutron ratio for the Am–Be neutron source. Appl Radiat Isot 2007; 65(12):1318–1321.

Mohan S, Chopra V. Biological effects of radiation. In: Dhoble S, Chopra V, Nayar V, Kitis G, Poelman D, Swart H, eds. Radiation Dosimetry Phosphors. Woodhead Publishing, 2022:485– 508.

Mortazavi SMJ, Kardan M, Sina S, Baharvand H, Sharafi N. Design and fabrication of high density borated polyethylene nanocomposites as a neutron shield. Int J Radiat Res 2016; 14(4).

Neville AM. Properties of concrete. 5th ed. Harlow: Pearson Education Limited, 2011.

Niita K, Sato T, Iwase H, Nose H, Nakashima H, Sihver L. PHITS—a particle and heavy ion transport code system. Radiat Meas 2006; 41(9-10):1080– 1090.

Nurhadiansyah N, Kim J. Monte Carlo simulation of shielding materials in storage drums for 241Am-Be disused sealed radioactive sources. J Radiat Res Appl Sci 2024; 17:101109.

Ogawa T. Prediction of composite neutron source spectra by combination of JENDL-5 and PHITS. Ann Nucl Energy 2025; 216:111256.

Qi Z, Yang Z, Li J, Guo Y, Yang G, Yu Y, Zhang J. The advancement of neutron-shielding materials for the transportation and storage of spent nuclear fuel. Materials 2022; 15(9):3255.

Rilwan U, Abdulazeez M, Maina I, Olasoji O, El-Taher A, Alhindawy IG, Mahmoud K, Sayyed M, Elsafi M, Rashad M, Maghrbi Y. The use of coconut shell ash as partial replacement of cement to improve the thermal properties of concrete and waste management sustainability in Nigeria and Africa, for radiation shielding application. Sci Afr 2025; 27.

Sato T. Analytical model for estimating the zenith angle dependence of terrestrial cosmic ray fluxes. PLoS ONE 2016; 11(8):e0160390.

Sato T. EXPACS: Excel-based Program for calculating Atmospheric Cosmic-ray Spectrum User's Manual. Ibaraki: Japan Atomic Energy Agency, 2018.

Sato T, Iwamoto Y, Hashimoto S, Ogawa T, Furuta T, Abe SI, Kai T, Matsuya Y, Matsuda N, Hirata Y, Sekikawa T, Yao L, Tsai PE, Ratliff HN, Iwase H, Sakaki Y, Sugihara K, Shigyo N, Sihver L, Niita K. Recent improvements of the particle and heavy ion transport code system – PHITS version 3.33. J Nucl Sci Technol 2023; 61(1):127–135.

Taylor HFW. Cement chemistry. 2nd ed. London: Thomas Telford, 1997.

Ward GK, Millero FJ. The effect of pressure on the ionization of boric acid in aqueous solutions from molal-volume data. J Solution Chem 1974; 3(6):417– 430.

X-5 Monte Carlo Team. MCNP - Version 5, Vol. I: Overview and theory. Report LA-UR-03-1987. Los Alamos: Los Alamos National Laboratory, 2003.

Zeng C, Kang Q, Duan Z, Qin B, Feng X, Lu H, Lin Y. Development of polymer composites in radiation shielding applications: a review. J Inorg Organomet Polym 2023; 33:2191–2239.